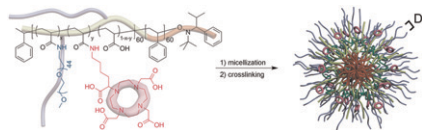
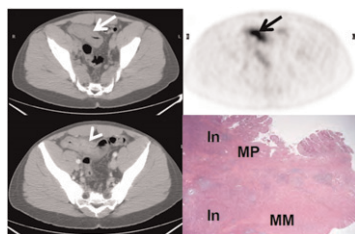


Focus on PET nanoparticles: Welch and colleagues highlight current approaches to and future challenges in the design of nanomaterials with optimized composition for tissue-selective PET imaging. **Page 1743**



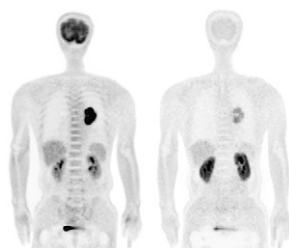
Quantitative studies of bone: Blake and colleagues provide perspective on current biochemical, radiographic, and radionuclide techniques for assessment of bone remodeling and preview a related article in this issue of *JNM*. **Page 1747**

PET/CT in obstructive Crohn disease: Jacene and colleagues explore the accuracy of PET/CT in identifying active inflammation in patients with Crohn disease before surgical resection for obstructive symptoms and discuss implications for improved management. **Page 1751**



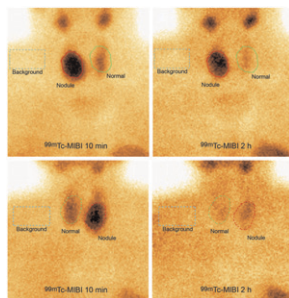
SUV and CT measurement reproducibility: Jacene and colleagues estimate and compare across different readers and institutions the reproducibility of ^{18}F -FDG PET standardized uptake values and CT size measurements in malignant tumors before and during therapy. **Page 1760**

^{18}F -FMT and lung cancer outcomes: Kaira and colleagues report on the prognostic abilities of this amino-acid tracer in PET assessment of primary tumors in patients with non-small cell lung cancer. **Page 1770**

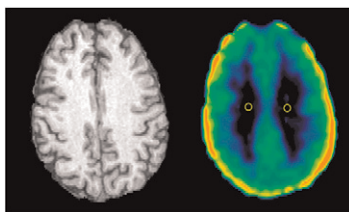


Monitoring liver metastasis response: Vriens and colleagues use dynamic contrast-enhanced MRI and ^{18}F -FDG PET to examine the relationship between functional tumor vasculature and tumor metabolism during chemotherapy in patients with colorectal liver metastases. **Page 1777**

$^{99\text{m}}\text{Tc}$ -MIBI and MRP1 in thyroid lesions: Saggiorato and colleagues investigate the usefulness of visual and semiquantitative analyses of $^{99\text{m}}\text{Tc}$ -MIBI scintigraphy for pre-operative characterization of thyroid nodules with indeterminate cytologic diagnoses and explore the associated relevance of P-glycoprotein/multidrug resistance-associated protein-1 expression. **Page 1785**



^{18}F -FCWAY PET in epilepsy: Giovacchini and colleagues report on the use of cerebral white matter as a reference region in ^{18}F -FCWAY PET detection of differences in

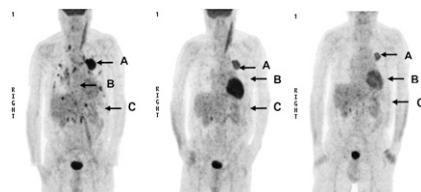


$5\text{-HT}_{1\text{A}}$ binding in patients with temporal lobe epilepsy and healthy controls. **Page 1794**

PET, neuroinflammation, and schizophrenia: Doorduyn and colleagues use ^{11}C -(*R*)-PK11195 PET to investigate the role of focal neuroinflammation during psychotic phases in patients with schizophrenia. **Page 1801**

^{18}F -fluoride PET in osteoporosis: Uchida and colleagues examine changes in regional bone remodeling and turnover measured by ^{18}F -fluoride PET, the relationship between these measured changes and conventional bone metabolism parameters, and the effects of bisphosphonate treatment. **Page 1808**

PET and everolimus treatment: Nogová and colleagues assess the utility of ^{18}F -FDG PET measurement of glucose metabolism inhibition as a pharmacodynamic marker in patients with everolimus-treated non-small cell lung cancer. **Page 1815**

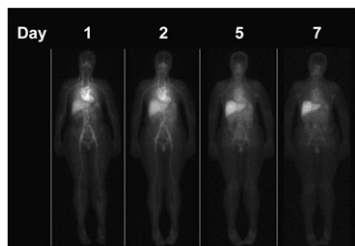


^{18}F -FDG uptake molecular correlates: Jadvar and colleagues provide an educational overview of current data on correlations between underlying molecular biology and clinical observations of tumor ^{18}F -FDG accumulation in human lung, breast, and colon cancers. **Page 1820**

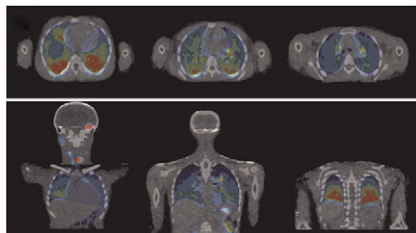
^{89}Zr -cmAb U36 immuno-PET: Börjesson and colleagues present first-in-human assessments of safety, biodistribution, radiation dose, and quantification of this ^{89}Zr -labeled chimeric monoclonal antibody in patients with head and neck squamous cell carcinoma. **Page 1828**

^{90}Y -ibritumomab dosimetry: Bischof Delaloye and colleagues document the radiation exposure associated with ^{90}Y -ibritumomab

tiuxetan when used as consolidation therapy in adults with low or minimal tumor burden after first-line therapy of advanced follicular lymphoma. **Page 1837**

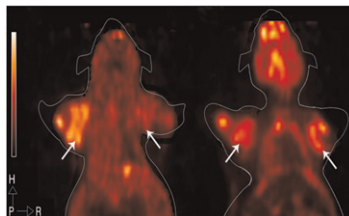


Real-time 3D-RD treatment planning: Hobbs and colleagues describe patient-specific 3D Monte Carlo-based dosimetry, with ^{124}I PET for pharmacokinetics, for ^{131}I treatment planning in a child with differentiated papillary thyroid cancer, lung involvement, and cerebral metastases. **Page 1844**

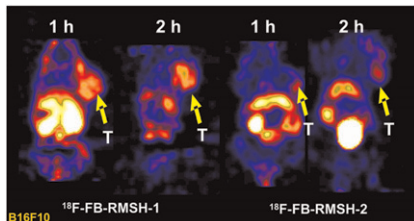


PET and trastuzumab response: McLarty and colleagues report on a mouse study designed to determine whether changes in ^{18}F -FDG uptake on PET can be associated with responses to trastuzumab treatment in breast cancer. **Page 1848**

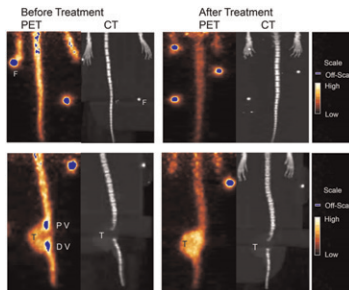
Dual-tracer PET in colorectal cancer: Hui and colleagues investigate whether ^{18}F -FDG and ^{18}F -FLT can be used complementarily in PET monitoring of the biologic characteristics of colorectal cancer and prediction of outcomes. **Page 1857**



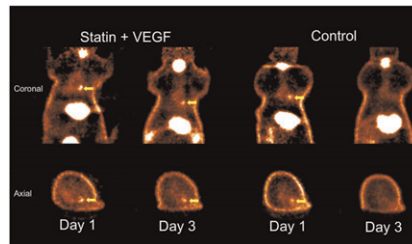
^{18}F metallopeptides for melanoma imaging: Ren and colleagues assess the utility of an ^{18}F -labeled probe for PET imaging of melanocortin type 1 receptor-positive malignant melanoma. **Page 1865**



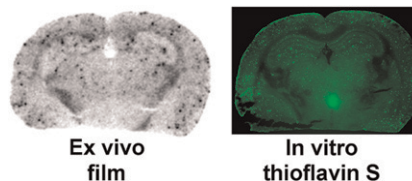
Imaging of osteolytic bone metastases: Wadas and colleagues describe the evaluation of a ^{64}Cu -labeled agent for imaging osteolytic bone metastases and associated inflammation by targeting the $\alpha_v\beta_3$ integrin on osteoclasts and proinflammatory cells involved at the bone metastatic site. **Page 1873**



Cell survival imaging after pretreatment: Higuchi and colleagues determine whether reporter gene PET can be used to detect the effects of atorvastatin and vascular endothelial growth factor on survival of endothelial progenitor cells after transplantation in the rat heart. **Page 1881**

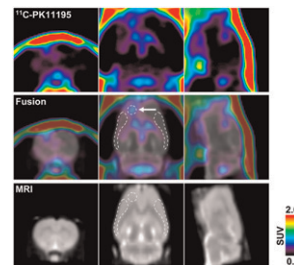


^{18}F -AV-45 and A β plaques: Choi and colleagues describe small-animal studies of the properties of this agent for PET imaging of β -amyloid as a biomarker of pathogenesis processes in Alzheimer disease. . . . **Page 1887**



A new ribonucleoside radiotracer: Zlatopolskiy and colleagues report on the synthesis and preclinical evaluation of IV-14, a ^{131}I -labeled ribonucleoside radiotracer, as a uridine-cytidine kinase-specific marker for tumor visualization. **Page 1895**

PET and neurogenic inflammation: Cui and colleagues describe a PET technique using ^{11}C -PK11195, a PET ligand for peripheral type-benzodiazepine receptors, to evaluate microglial activation in rat brain in an experimental model of migraine. **Page 1904**



ON THE COVER

A study was undertaken of the in vivo relationship between functional tumor vasculature, determined by dynamic contrast-enhanced MRI, and tumor metabolism, determined by dynamic ^{18}F -FDG PET, during cytotoxic treatment of patients with colorectal liver metastases. Cytotoxic chemotherapy was found not to alter the properties of tumor vasculature but to decrease glucose consumption by tumor cells.

See page 1780.

